



Data Article

Dataset of the crystal structures, electrical transport properties, and first-principles electronic structures of GeTe-rich GeTe-Sb₂Te₃ thermoelectric materials



Tomohiro Oku^{a,*}, Hiroki Funashima^b, Shogo Kawaguchi^c,
Yoshiki Kubota^a, Atsuko Kosuga^{a,d,**}

^a Department of Physical Science, Graduate School of Science, Osaka Prefecture University, Sakai, Osaka 599-8531, Japan

^b Department of Comprehensive Engineering, Kindai University Technical College, Mie, Nabari 518-0459, Japan

^c Diffraction and Scattering Division, Japan Synchrotron Radiation Research Institute (JASRI), Sayo-gun, Hyogo 679-5198, Japan

^d Japan Science and Technology Agency (JST), PRESTO, Kawaguchi, Saitama 332-0012, Japan

ARTICLE INFO

Article history:

Received 15 September 2021

Revised 3 October 2021

Accepted 5 October 2021

Available online 9 October 2021

Keywords:

Germanium telluride

First-principles calculation

Rietveld refinement

Ge defect

Synchrotron X-ray powder diffraction

Data description

ABSTRACT

The data presented in this article relate to the research article entitled “Superior room-temperature power factor in GeTe systems via multiple valence band convergence to a narrow energy range” [T. Oku et al., *Mater. Today Phys.* 20 (2021) 100484 (10.1016/j.mtphys.2021.100484)]. Polycrystalline (GeTe)_nSb₂Te₃ ($n = 10, 12, 16, 20,$ and 24) bulk samples were prepared by melting and annealing. The Ge defect concentration of each composition was estimated from Rietveld refinement of the synchrotron X-ray powder diffraction patterns. Electrical properties, such as the electrical resistivity and Seebeck coefficient, were measured from three specimens of each composition to confirm reproducibility. Electronic-band-structure parameters and electronic density-of-states of each composition were obtained by first-principles calculations.

DOI of original article: [10.1016/j.mtphys.2021.100484](https://doi.org/10.1016/j.mtphys.2021.100484)

* Corresponding author.

** Corresponding author at: Department of Physical Science, Graduate School of Science, Osaka Prefecture University, Sakai, Osaka 599-8531, Japan.

E-mail addresses: s_t.oku@p.s.osakafu-u.ac.jp (T. Oku), a-kosuga@p.s.osakafu-u.ac.jp (A. Kosuga).

<https://doi.org/10.1016/j.dib.2021.107462>

2352-3409/© 2021 The Author(s). Published by Elsevier Inc. This is an open access article under the CC BY license (<http://creativecommons.org/licenses/by/4.0/>)

Specifications Table

Subject	Materials Science
Specific subject area	crystal structure, band structure, and electrical properties of GeTe-Sb ₂ Te ₃ thermoelectric materials
Type of data	Table Figure
How data were acquired	Synchrotron X-ray powder diffraction (SXRPD) patterns were acquired (BL02B2 beamline, SPring-8, Japan). Rietveld refinement (RIETAN-FP) of SXRPD patterns was used to determine crystal structure parameters. The Ge defect concentration was estimated from Rietveld refinement by fixing the Ge site occupancy at certain intervals and varying the scale factor and lattice constants. Electrical properties were measured by Seebeck coefficient and electrical resistivity measurements (ZEM-3, Advance-RIKO Inc., Japan) and Hall measurements (ResiTest8400LRJ, TOYO Corp., Japan). Thermogravimetric/differential thermal analysis (TG-DTA; TG/DTA7200, SII NanoTechnology Inc., Japan). Electronic band structure and electronic density-of-states were determined by first-principles calculations with AkaiKKR using the Korringa-Kohn-Rostoker method within coherent-potential approximation (KKR-CPA).
Data format	Raw Analyzed Filtered
Parameters for data collection	Materials: polycrystalline (GeTe) _n Sb ₂ Te ₃ ($n = 10, 12, 16, 20,$ and 24) bulk samples Synthesis: melt at 1173 K overnight, anneal at 773 K for 10 days, water-quench SXRPD: 300 K, 400 K, 500 K, 600 K, and 700 K AkaiKKR calculation: GGA-PBE, semi-relativistic with spin-orbit interactions, high-quality k -mesh
Description of data collection	The crystal structure parameters, Ge defect concentration, electrical properties, electronic band structure parameters, and electronic density-of-states were determined for each composition of polycrystalline (GeTe) _n Sb ₂ Te ₃ ($n = 10, 12, 16, 20,$ and 24). Three specimens of each composition were used for electrical property measurements. The SXRPD patterns were normalized by the largest peak for each composition.
Data source location	Institution: Osaka Prefecture University City/Town/Region: Sakai, Osaka Country: Japan
Data accessibility	With the article
Related research article	T. Oku, H. Funashima, S. Kawaguchi, Y. Kubota, A. Kosuga, Superior room-temperature power factor in GeTe systems via multiple valence band convergence to a narrow energy range, Mater. Today Phys. 20 (2021) 100484. 10.1016/j.mtphys.2021.100484

Value of the Data

- Information on the crystal structure and Ge defect concentration provides a deep understanding of the electronic band structure and electronic transport properties of this material system.
- These data are beneficial to researchers who are interested in the crystal structure, Ge defect concentration, band structure parameters, and electrical transport properties of GeTe derivatives.

- These data provide new insights to improve the thermoelectric properties of GeTe derivatives in terms of defect structure engineering and band engineering. These data also provide useful information on functional materials with respect to crystal structure, high-temperature stability, electronic band structure, and electronic transport properties.

1. Data Description

The data presented in this article are in reference to the research article entitled “Superior room-temperature power factor in GeTe systems via multiple valence band convergence to a narrow energy range” [1]. All the numerical datum referred to in this section are also available as supplementary data files.

Table 1 lists previously reported crystal structures of polycrystalline $(\text{GeTe})_n\text{Sb}_2\text{Te}_3$ bulk samples with various n and prepared by various heat treatments.

Fig. 1a and b show the enlarged SXRPD patterns of $(\text{GeTe})_n\text{Sb}_2\text{Te}_3$ ($n = 16$ and 24 , respectively) from 5° to 13° . The triangle symbols represent Ge peaks. These peaks are ascribed to the presence of Ge defects of $(\text{GeTe})_n\text{Sb}_2\text{Te}_3$ ($n = 16$ and 24). Ge peaks were observed for all compositions. Fig. 1c shows the results of Rietveld analysis of $(\text{GeTe})_n\text{Sb}_2\text{Te}_3$ ($n = 10, 12, 16, 20$, and 24) to estimate the amounts of Ge defects, and Fig. 1d shows an enlarged view of the region near the origin. The horizontal axis ($-\Delta g$) shows the amount of change of Ge site occupancy; Δg is expressed as $g - g_i$, where g is the Ge site occupancy and g_i is the initial value of Ge site occupancy. g_i is calculated from the Ge content in the formula of $(\text{GeTe})_n\text{Sb}_2\text{Te}_3$ ($n = 10, 12, 16, 20$, and 24); for example, in the case of $n = 12$, g_i is set as 0.8 . An increase in the value of the horizontal axis ($-\Delta g$) indicates that the Ge defect concentration increases. The vertical axis (ΔR_{wp}) shows the amount of change in the reliability factor R_{wp} , at the minimum value of which (g_{min}), the Ge defect concentration is regarded as the best reflection of the experimental value. ΔR_{wp} is expressed as $(R_{\text{wp}})_g - (R_{\text{wp}})_i$, where $(R_{\text{wp}})_g$ represents R_{wp} at a certain g , and $(R_{\text{wp}})_i$ represents R_{wp} at g_i . The curves in the figure are quadratic functions fitted by the least-squares method. ΔR_{wp} shows minimum values at $g = 0.764$ for $n = 10$; $g = 0.797$ for $n = 12$;

Table 1

Relationship between the crystal structure and heat treatment of polycrystalline $(\text{GeTe})_n\text{Sb}_2\text{Te}_3$ bulk materials (as previously reported).

n in $(\text{GeTe})_n\text{Sb}_2\text{Te}_3$	Crystal structure	Heat treatment	Authors
3	$R\bar{3}m$	1. Anneal (500–550 °C, 2 days)	Rosenthal et al. [2]
7	$R\bar{3}m$	2. Water-quench	
12	$R\bar{3}m$		
14	$R\bar{3}m$		
17	$R\bar{3}m$		
9	$R\bar{3}m$	1. Anneal (773 K, 3 days) 2. SPS (773 K, 5 min)	Chen et al. [3]
7	-	1. Anneal (1223 K, 2 h)	Xu et al. [4]
12	-	2. Water-quench	
14	-	3. Anneal (873 K, 2/4/7 h)	
17	$R\bar{3}m$	4. Water quench	
19	-	5. SPS (823 K, 5 min)	
18	$Fm\bar{3}m$	6. Anneal 7. Water-quench 8. SPS	Xu et al. [5]
10	$Fm\bar{3}m$	1. Anneal (773 K, 10 days)	This work
12	$R\bar{3}m$	2. Water-quench	
16	$R\bar{3}m$		
20	$R\bar{3}m$		
24	$R\bar{3}m$		

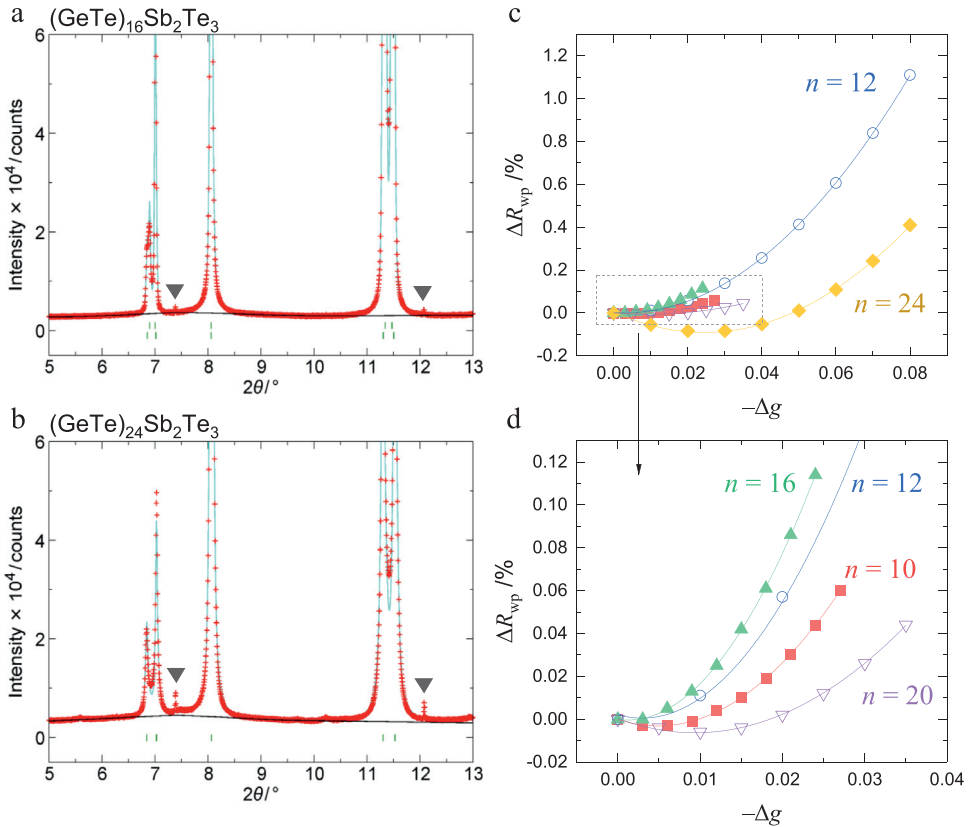


Fig. 1. Enlarged synchrotron X-ray powder diffraction (SXRPD) patterns at 5° – 13° for $(\text{GeTe})_n\text{Sb}_2\text{Te}_3$ with (a) $n = 16$ and (b) $n = 24$. The triangle symbols represent Ge peaks. (c) Amount of change in the reliability factor (ΔR_{wp}) as a function of the amount of change in the Ge site occupancy ($-\Delta g$) for $(\text{GeTe})_n\text{Sb}_2\text{Te}_3$ ($n = 10, 12, 16, 20$, and 24). Here, ΔR_{wp} is expressed as $(R_{wp})_g - (R_{wp})_i$, where $(R_{wp})_g$ represents R_{wp} at a certain g , and $(R_{wp})_i$ represents R_{wp} at g_i . g is the Ge site occupancy, Δg is expressed as $g - g_i$, where g is the Ge site occupancy, and g_i is the initial value of the Ge site occupancy. (d) Enlarged image of the dotted area in (c).

$g = 0.841$ for $n = 16$; $g = 0.860$ for $n = 20$; and $g = 0.864$ for $n = 24$. This corresponds to Ge defect concentrations ($g_i - g_{\min}$) of 0.5% for $n = 10$; 0.3% for $n = 12$; 0.1% for $n = 16$; 0.9% for $n = 20$; and 2.4% for $n = 24$.

Fig. 2 shows the thermogravimetric-differential thermal analysis (TG-DTA) results of $(\text{GeTe})_{12}\text{Sb}_2\text{Te}_3$. Endothermic reactions occur approximately at 600 and 750 K. The melting point of $(\text{GeTe})_{12}\text{Sb}_2\text{Te}_3$ is in the 950–1000 K range.

Fig. 3 shows the high-temperature SXRPD data of $(\text{GeTe})_{12}\text{Sb}_2\text{Te}_3$. These data mainly entail the rhombohedral structure ($R3m$) and cubic structure ($Fm\bar{3}m$) of GeTe at and below 500 K. Some peaks other than those of the main phases appeared at and above 600 K.

Fig. 4 presents the temperature-dependent electrical properties, such as the Seebeck coefficient S , electrical resistivity ρ , and power factor $S^2\rho^{-1}$ of $(\text{GeTe})_n\text{Sb}_2\text{Te}_3$ ($n = 10, 12, 16, 20$, and 24). These properties were measured using three specimens per composition to confirm the reproducibility. The filled area in Fig. 4 denotes the data range from a maximum value to minimum value. Measurement errors were not plotted in this figure. The actual values of each lot sample are included in the supplementary material.

Table 2 lists the detailed band structure parameters of $(\text{GeTe})_n\text{Sb}_2\text{Te}_3$ ($n = 10, 12, 16, 20$, and 24), GeTe-10, and GeTe-12. Here, GeTe-10 and GeTe-12 have the composition of GeTe and the

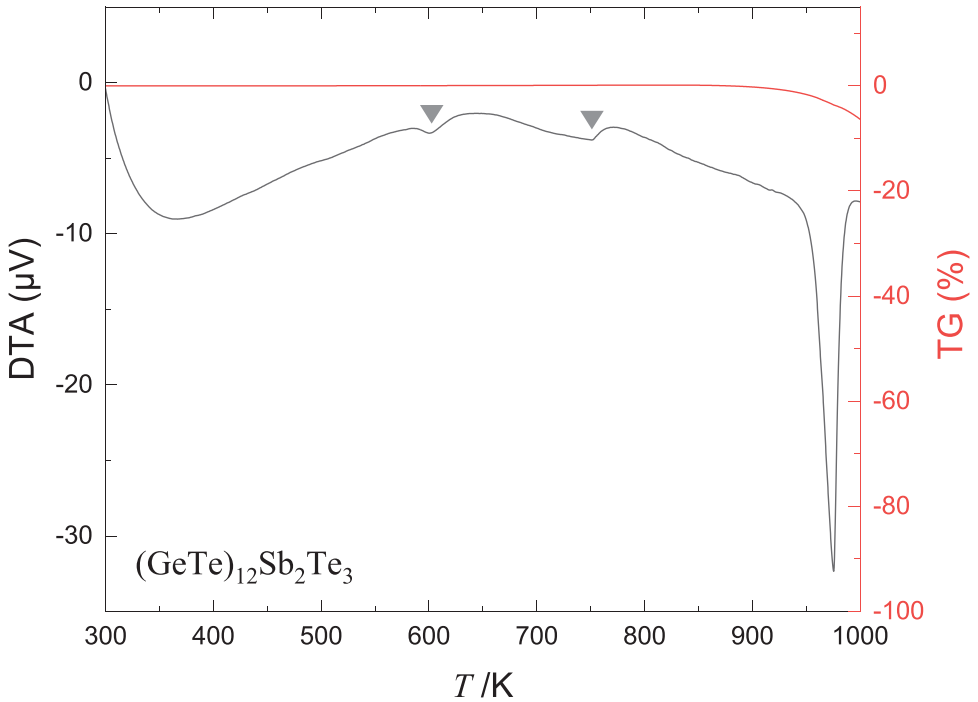


Fig. 2. Thermogravimetric-differential thermal analysis (TG-DTA) of $(\text{GeTe})_{12}\text{Sb}_2\text{Te}_3$. The triangles indicate the peak positions of the endothermic reaction.

Table 2

Detailed band structure parameters of $(\text{GeTe})_n\text{Sb}_2\text{Te}_3$ ($n = 10, 12, 16, 20,$ and 24), GeTe-10, and GeTe-12. E_{VB} (VB = L, Σ , Δ , Z, L, Σ , Σ' , and Δ') imply the energy at the valence band maximum of each band, VB. E_{F} denotes the Fermi level derived from the experimental hole concentration, n_{H} , at room temperature (approximately 300 K). E_{g} is the band gap energy. GeTe-10 and GeTe-12 denote the materials with the composition GeTe with the same lattice constants and atomic coordinates as those of $(\text{GeTe})_{10}\text{Sb}_2\text{Te}_3$ and $(\text{GeTe})_{12}\text{Sb}_2\text{Te}_3$, respectively.

$Fm\bar{3}m$	E_{L}/eV	E_{Σ}/eV	E_{Δ}/eV	E_{F}/eV	E_{g}/eV		
$(\text{GeTe})_{10}\text{Sb}_2\text{Te}_3$	-0.01	-0.06	-0.19	-0.24	0.04		
GeTe-10	-0.09	-0.16	-0.35	-0.28	0.18		
$R3m$	E_{Z}/eV	E_{L}/eV	E_{Σ}/eV	$E_{\Sigma'}/\text{eV}$	$E_{\Delta'}/\text{eV}$	E_{F}/eV	E_{g}/eV
$(\text{GeTe})_{12}\text{Sb}_2\text{Te}_3$	-0.16	-0.19	-0.23	-0.10	-0.24	-0.28	0.20
$(\text{GeTe})_{16}\text{Sb}_2\text{Te}_3$	-0.15	-0.15	-0.24	-0.13	-0.27	-0.32	0.21
$(\text{GeTe})_{20}\text{Sb}_2\text{Te}_3$	-0.20	-0.22	-0.34	-0.14	-0.33	-0.36	0.28
$(\text{GeTe})_{24}\text{Sb}_2\text{Te}_3$	-0.21	-0.21	-0.35	-0.13	-0.34	-0.37	0.37
GeTe-12	-0.18	-0.18	-0.29	-0.14	-0.36	-0.29	0.40

same lattice parameters and atomic coordinates as those of $(\text{GeTe})_{10}\text{Sb}_2\text{Te}_3$ and $(\text{GeTe})_{12}\text{Sb}_2\text{Te}_3$, respectively. The GeTe systems calculated here have a face-centered cubic (fcc) structure with space group $Fm\bar{3}m$, or rhombohedral structure with space group $R3m$. The cubic structures have valence band maximums (VBMs) near the Fermi level at the L band, Σ band, and Δ band. Similarly, the VBMs of the rhombohedral structures are the Z band, L band, Σ band, Σ' band, and Δ' band. The symbol with a prime ($'$), which appears in the rhombohedral structure, represents an axis in which the three-fold rotational symmetry is lost because of the reduced symmetry.

Fig. 5 shows the total density of states and Sb partial density of states (s and p) near the Fermi energy of $(\text{GeTe})_n\text{Sb}_2\text{Te}_3$ ($n = 10, 12, 16, 20,$ and 24).

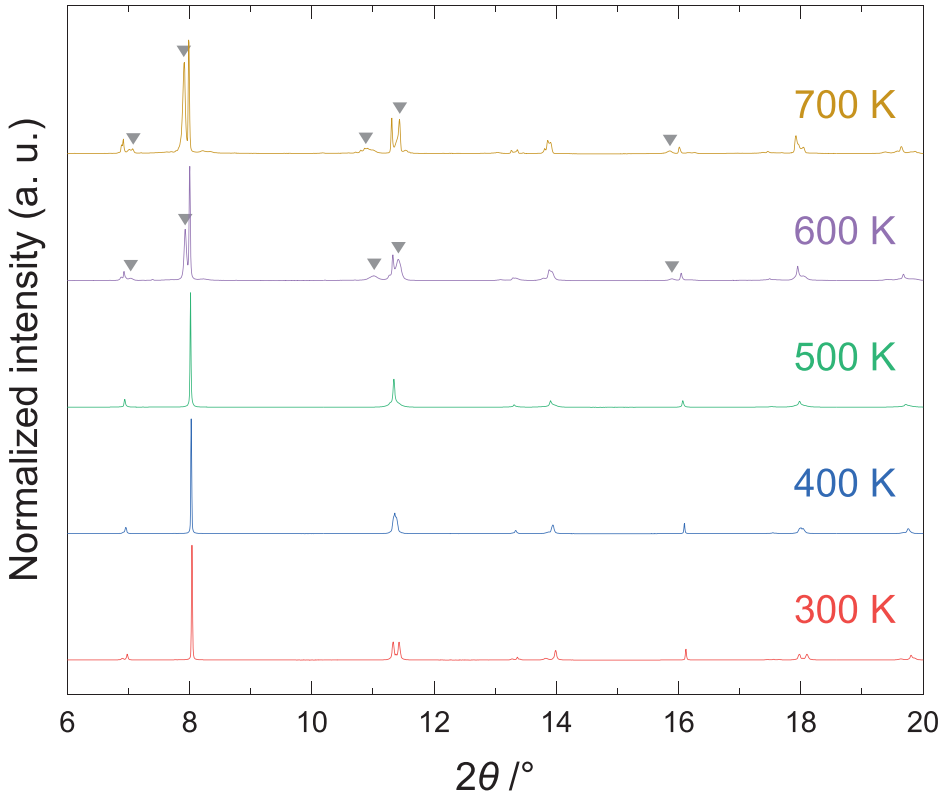


Fig. 3. High-temperature synchrotron X-ray powder diffraction (SXRPD) patterns of $(\text{GeTe})_n\text{Sb}_2\text{Te}_3$. The triangles indicate peaks other than those of the main phase.

2. Experimental Design, Materials and Methods

We synthesized polycrystalline $(\text{GeTe})_n\text{Sb}_2\text{Te}_3$ bulk samples ($n = 10, 12, 16, 20,$ and 24) by melting and annealing. First, stoichiometric Ge, Sb, and Te were melted in vacuumed silica tubes at 1173 K overnight and furnace-cooled. Then, the cooled ingots were annealed at 773 K for 10 days followed by water quenching.

Synchrotron X-ray powder diffraction (SXRPD), thermogravimetric-differential thermal analysis (TG-DTA), Seebeck coefficient/electrical resistivity measurements, and Hall measurements were employed. For SXRPD, we used the BL02B2 beamline at the Japan Synchrotron Radiation Research Institute, SPring-8, with a Debye–Scherrer diffractometer [6]. Powder samples crushed from the ingots and CeO_2 standard powder were placed in glass capillary tubes with a diameter of 0.2 mm for the refinement of X-ray wavelength. Measurements were performed at temperatures of 300, 400, 500, 600, and 700 K. We determined the crystal structures of the samples from their diffraction patterns by Rietveld refinement with RIETAN-FP [7]. Here, we also quantified the Ge defect concentration by fixing the value of the Ge site occupancy at a certain interval and varying that of the scale factor and lattice constants. TG-DTA was performed using a TG/DTA7200 instrument (SII NanoTechnology Inc., Japan) under N_2 gas flow. The Seebeck coefficient S , and electrical resistivity ρ , were measured using a ZEM-3 instrument (Advance-RIKO Inc., Kanagawa, Japan) in the temperature range of room temperature (approximately 300 K) to 723 K. Here, the power factor $S^2\rho^{-1}$, was calculated using the obtained S and ρ . This measurement was performed with three samples of each $(\text{GeTe})_n\text{Sb}_2\text{Te}_3$ variant. Hall carrier density and

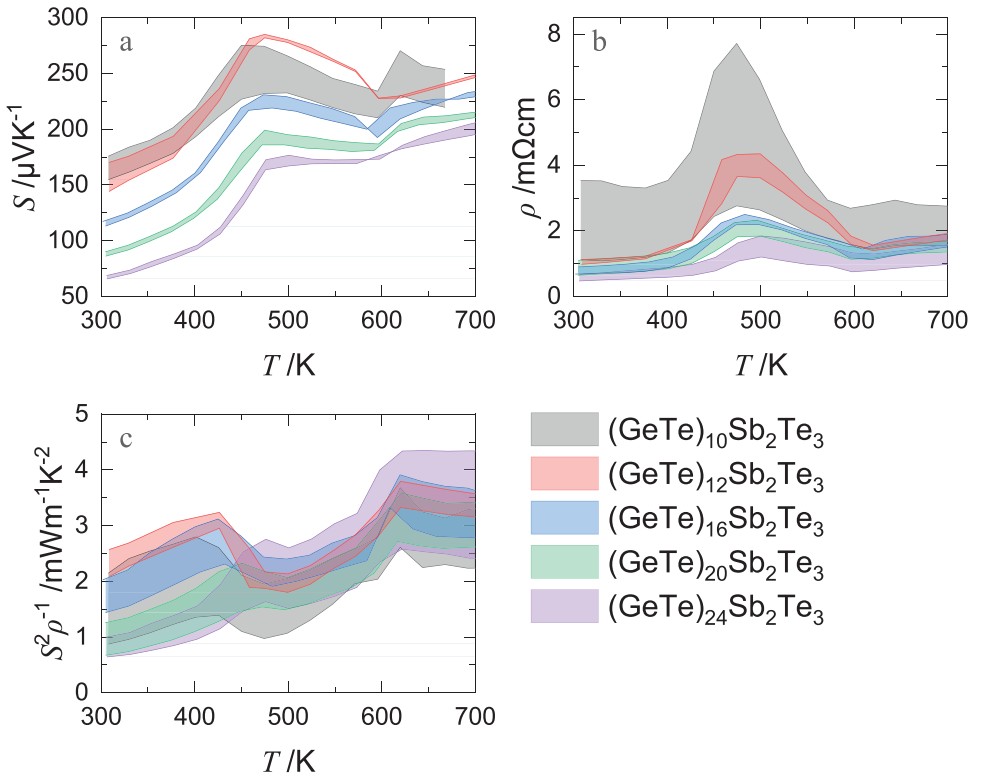


Fig. 4. Temperature-dependence of (a) Seebeck coefficient S , (b) electrical resistivity ρ , and (c) power factor $S^2\rho^{-1}$, of multiple lot samples of $(\text{GeTe})_n\text{Sb}_2\text{Te}_3$ ($n = 10, 12, 16, 20,$ and 24) to confirm reproducibility. The areas between the minimum and maximum measured values for multiple samples are filled in for each composition. Measurement error bars of single samples are not plotted in this figure.

Hall carrier mobility were measured using a ResiTest8400LRJ instrument (TOYO Corp., Tokyo, Japan) at room temperature.

We conducted first-principles calculations by using the refined structure parameters of $(\text{GeTe})_n\text{Sb}_2\text{Te}_3$ as input parameters for model-based calculations. The calculation was also performed for GeTe-10 and GeTe-12, which have the composition of GeTe and the same lattice parameters and atomic coordinates as those of $(\text{GeTe})_{10}\text{Sb}_2\text{Te}_3$ and $(\text{GeTe})_{12}\text{Sb}_2\text{Te}_3$, respectively. The programming package AkaiKKR was used for first-principles calculations, which applies the Korringa-Kohn-Rostoker method within coherent-potential approximation (KKR-CPA) [8]. The exchange and correlation potentials were constructed by the generalized gradient approximation with Perdew-Burke-Ernzerhof parameterization (GGA-PBE) [9,10]. Self-consistent field calculations were semi-relativistic, with spin-orbit interactions, in a high-quality Brillouin zone mesh. We calculated the electronic density-of-states (DOS) and evaluated the band structure parameters: E_{VB} , energy at the valence band maximums of each band VB; E_{F} , Fermi level; and E_{g} , band gap energy. E_{F} was derived from the experimental n_{H} value according to the definition of carrier concentration.

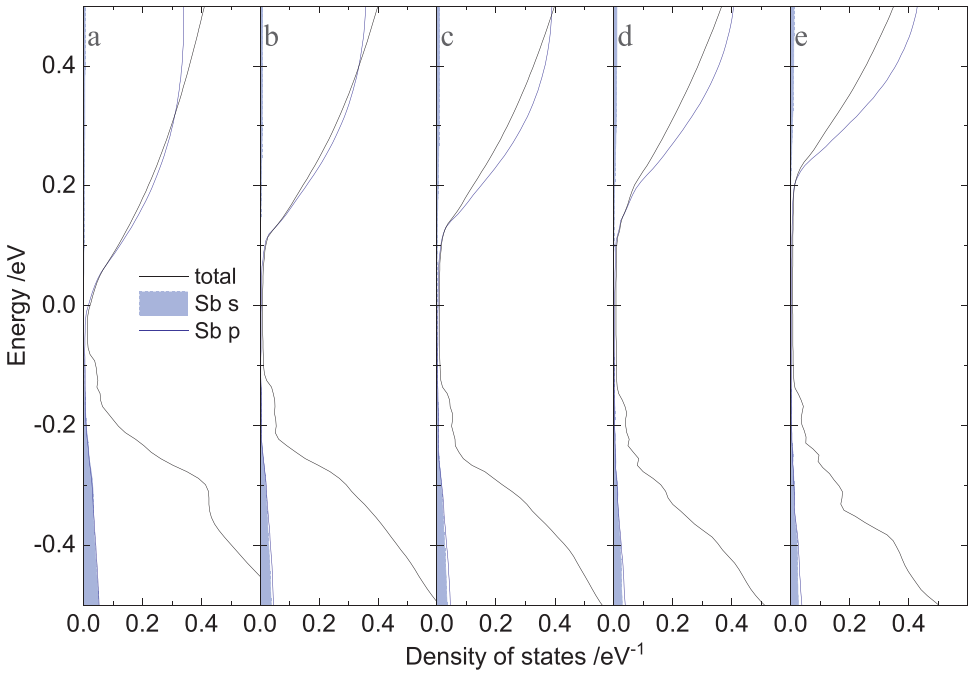


Fig. 5. Total density of states and Sb partial density of states (*s* and *p*) near the Fermi energies of $(\text{GeTe})_n\text{Sb}_2\text{Te}_3$ with (a) $n = 10$, (b) $n = 12$, (c) $n = 16$, (d) $n = 20$, and (e) $n = 24$.

Ethics Statement

The authors declare compliance with the publication code of ethics of this journal.

Funding

This work was supported by JST PRESTO (Grant Number JPMJPR17R4), Japan; the Thermal & Electric Energy Technology Foundation, Japan; and Tanikawa fund promotion of thermal technology, Japan.

Declaration of Competing Interest

The authors declare that they have no known competing financial interests or personal relationships that could have appeared to influence the work reported in this paper.

CRediT Author Statement

Tomohiro Oku: Validation, Formal analysis, Investigation, Writing – original draft, Visualization; **Hiroki Funashima:** Software, Validation, Formal analysis, Resources; **Shogo Kawaguchi:** Investigation, Resources; **Yoshiki Kubota:** Investigation, Resources; **Atsuko Kosuga:** Conceptualization, Formal analysis, Writing – review & editing, Resources, Supervision, Project administration, Funding acquisition.

Acknowledgments

We would like to thank Mr. Hiroki Nishizaki, Ms. Yuka Ohkita, and Ms. Mie Ando for helping us with the sample preparation and experimental evaluation. Synchrotron radiation experiments were performed at SPring-8 with the approval of the Japan Synchrotron Radiation Research Institute (JASRI, Proposal No. 2017A1464, 2018A0074, 2018B0074, and 2019A1463).

Supplementary Materials

Supplementary material associated with this article can be found in the online version at doi:[10.1016/j.dib.2021.107462](https://doi.org/10.1016/j.dib.2021.107462).

References

- [1] T. Oku, H. Funashima, S. Kawaguchi, Y. Kubota, A. Kosuga, Superior room-temperature power factor in GeTe systems via multiple valence band convergence to a narrow energy range, *Mater. Today Phys.* 20 (2021) 100484, doi:[10.1016/j.mtphys.2021.100484](https://doi.org/10.1016/j.mtphys.2021.100484).
- [2] T. Rosenthal, M.N. Schneider, C. Stiewe, M. Döblinger, O. Oeckler, Real structure and thermoelectric properties of GeTe-rich germanium antimony tellurides, *Chem. Mater.* 23 (2011) 4349–4356, doi:[10.1021/cm201717z](https://doi.org/10.1021/cm201717z).
- [3] S. Chen, H. Bai, J. Li, W. Pan, X. Jiang, Z. Li, Z. Chen, Y. Yan, X. Su, J. Wu, C. Uher, X. Tang, Vacancy-based defect regulation for high thermoelectric performance in $\text{Ge}_9\text{Sb}_2\text{Te}_{12-x}$ compounds, *ACS Appl. Mater. Interfaces* 12 (2020) 19664–19673, doi:[10.1021/acsami.0c02155](https://doi.org/10.1021/acsami.0c02155).
- [4] X. Xu, L. Xie, Q. Lou, D. Wu, J. He, Boosting the thermoelectric performance of pseudo-layered $\text{Sb}_2\text{Te}_3(\text{GeTe})_n$ via vacancy engineering, *Adv. Sci.* 5 (2018) 1801514, doi:[10.1002/advs.201801514](https://doi.org/10.1002/advs.201801514).
- [5] X. Xu, Y. Huang, L. Xie, D. Wu, Z. Ge, J. He, Realizing improved thermoelectric performance in Bi_{13} -doped $\text{Sb}_2\text{Te}_3(\text{GeTe})_{17}$ via introducing dual vacancy defects, *Chem. Mater.* 32 (2020) 1693–1701, doi:[10.1021/acs.chemmater.0c00113](https://doi.org/10.1021/acs.chemmater.0c00113).
- [6] S. Kawaguchi, M. Takemoto, K. Osaka, E. Nishibori, C. Moriyoshi, Y. Kubota, Y. Kuroiwa, K. Sugimoto, High-throughput powder diffraction measurement system consisting of multiple MYTHEN detectors at beamline BL02B2 of SPring-8, *Rev. Sci. Instrum.* 88 (2017) 085111, doi:[10.1063/1.4999454](https://doi.org/10.1063/1.4999454).
- [7] F. Izumi, K. Momma, Three-dimensional visualization in powder diffraction, *Solid State Phenom.* 130 (2007) 15–20, doi:[10.4028/www.scientific.net/SSP.130.15](https://doi.org/10.4028/www.scientific.net/SSP.130.15).
- [8] H. Akai, Fast Korringa-Kohn-Rostoker coherent potential approximation and its application to FCC Ni-Fe systems, *J. Phys. Condens. Matter* 1 (1989) 8045–8064, doi:[10.1088/0953-8984/1/43/006](https://doi.org/10.1088/0953-8984/1/43/006).
- [9] J.P. Perdew, J.A. Chevary, S.H. Vosko, K.A. Jackson, M.R. Pederson, D.J. Singh, C. Fiolhais, Atoms, molecules, solids, and surfaces: applications of the generalized gradient approximation for exchange and correlation, *Phys. Rev. B* 46 (1992) 6671–6687, doi:[10.1103/PhysRevB.46.6671](https://doi.org/10.1103/PhysRevB.46.6671).
- [10] J.P. Perdew, K. Burke, M. Ernzerhof, Generalized gradient approximation made simple, *Phys. Rev. Lett.* 77 (1996) 3865–3868, doi:[10.1103/PhysRevLett.77.3865](https://doi.org/10.1103/PhysRevLett.77.3865).